Appendix O: Rim Joint Assessment

1 Overview

The primary objective of the main report has been to address the fracture and fatigue integrity of the circumferential welds in petroleum road fuel tankers manufactured by GRW. However, in light of findings that resulted from the topple testing of non-compliant GRW tankers by HSL, additional investigation of the welds joining the extrusion bands to the bulkheads (ie the so-called "rim joint welds") has been required.

This appendix is concerned with the assessment of these rim joint welds and involves both metallographic examinations and numerical analyses.

2 Objective

- To examine the rim joints from the topple tested tanks J3910 and J2580 and to provide numerical analysis to explain the failures.

3 Metallographic Examination of Rim Joints

3.1 Overview

After the topple testing of both J3910 and J2580, apparent ruptures in the vicinity of the rim joint were observed. For J3910, the ruptures appeared on the front end dish along the rim joint weld toe at the ends of the bulge that formed on the flattened side. For J2580, a rupture appeared through the weld throat of the rim joint weld on the rear end dish. In order to investigate the cause of these ruptures, sections of the appropriate end dishes from J3910 and J2580 were provided to TWI for further metallographic examination.

3.2 Examination of J3910

The section of end dish removed from J3910 after topple testing is shown in Figure O1 as-received by TWI. In this figure, the apparent cracking of the bulkhead at either end of the bulge can be observed. The section was sampled at three locations as illustrated in Figure O2:

- Three samples were removed from location 1. This location contained the apparent through-wall rupture of the bulkhead and the samples were taken 50mm apart from each other.
- Two samples were removed from location 2. This location was positioned half-way along the flattened portion of the section where there were no observable cracks.
- Three samples were removed from location 3. At this location, similar to location 1, there was an apparent through-wall rupture of the bulkhead. The samples were taken 50mm apart from each other.

In Figure O3, the macrographs of the samples prepared from location 1 are shown. All three samples show evidence of cracking. Sample 1-A shows less in-plane bending than samples 1-B and 1-C, but exhibits a through-wall crack. Samples 1-B and 1-C show increasing levels of in-plane bending and cracks (but not through-wall cracks) initiating on the inner surface of the bulkhead. The cracks are orientated approximately 45^{o} to the principal in-plane bending stress, which is evidence of the onset of a shear failure. In all of these samples taken from location 1, the cracks initiate on the inner surface of the bulkhead at a location approximately 4-5mm offset from the toe of the rim joint weld on the inner surface of the bulkhead.

In Figure O4, the macrographs of the samples prepared from location 2 are presented. In these figures, the total level of in-plane bending is larger than that observed in the samples from location 1. However, no evidence of cracking can be seen.

Finally, in Figure O5, the macrographs of the samples prepared from location 3 are shown. Similar to the macrographs from location 1 (but in opposite order, moving from the position closest to the centre of the flattened portion outwards), sample 3-A shows the most in-plane bending, and sample 3-C shows the least in-plane bending. In all samples, the crack has initiated on the inner surface of the bulkhead and torn through the entire wall thickness of the bulkhead. The crack path in sample 3-A is more complex than previous samples, but appears to show that the crack initiated on the inner surface and tore at a 45^{o} angle to the principal bending stress. Once the crack reached the neutral axis of the bulkhead under bending (which can be seen due to the etching and polishing as a slightly darker region), the crack propagation changed direction under the action of an additional membrane loading until it tore the through the remainder of the bulkhead.

3.3 Examination of J2580

The section of end dish removed from J2580 after topple testing is shown in Figure O6 as-received by TWI. Examination of the rim joint was performed in a similar manner to that of J3910, with samples taken from three different locations along the length of the flattened portion.

In Figure O7, macrographs of the three samples prepared from location 1 are shown. Due to previous cuts that were made to facilitate the metallographic examination of the circumferential welds, parts of these samples are missing. However, from the remnant material, the cracking of the rim joint weld is clearly evident. In contrast to the samples from J3910 that showed cracking only in the bulkhead, in each of these samples, the rim joint weld throat has ruptured.

In Figure O8, macrographs of the two samples prepared from location 2 are presented. Similar to J3910, these samples were taken from the centre of the flattened portion and exhibit the largest amount of in-plane bending whilst not exhibiting any signs of cracking on the bulkhead. The macrograph for sample 2-B shows that there was a lack-of-fusion flaw with the dished end, extending for approximately 3.0mm from the root of the rim joint weld. Whilst the deformation due to topple testing prevents a clear visualisation of the original fit-up between the bulkhead and the extrusion band, the inclination of the slot in the extrusion indicates that the original parts were positioned so that the opening was less than 90^{o}. This might have contributed to the lack of fusion because of the restricted access to the root. Additional micrographs taken of the root of the rim joint weld provide a plausible explanation for the weld throat rupture in J2580. Figure O9 shows a micrograph taken from the location indicated by the red circle in Figure O8. There is an apparent remnant of a previous weld bead as outlined in the right frame of Figure O9. This could indicate that this section was located at a start/stop or overlap position. Such a location would have increased the likelihood of lack of fusion. Thus, the combination of a weld start/stop position and a potentially poor fit-up between the bulkhead and extrusion contributed to a 3.0mm lack of fusion flaw at the weld root of the rim joint. The in-plane bending action of the bulkhead during topple testing could have led to the propagation of this defect and rupture of the weld throat observed in the samples prepared from J2580.

Finally, in Figure O10, the three macrographs taken of samples prepared from location 3 are presented. Whilst the previous machining of samples at location 1 prevented images being taken of the weld root, the samples from location 3 clearly exhibit cracking that initiated at the lack of fusion flaw at the root of the rim joint weld. Additionally, the cracking of the circumferential weld (discussed in the main report) can also be seen in these macrographs.

3.4 Discussion

Metallographic examination of the rim joint welds from the sections received from J3910 and J2580 after topple testing resulted in the following observations:

- The samples from J3910 taken from the ends of the flattened portion showed through-wall cracking of the bulkhead. Each of the samples prepared from locations 1 and 3 showed crack initiation on the inner surface of the bulkhead. No other cracking of the rim joint weld was observed. The macrographs prepared from the centre of the flattened portion exhibited the largest in-plane bending but showed no evidence of cracking.
- The samples from J2580 showed cracking through the rim joint weld throat. Closer inspection of sample 2-B revealed a lack of fusion defect approximately 3.0mm long at the root of the rim joint weld. This lack of fusion defect was most likely due to the combination of a weld start/stop position and the poor fit-up between the bulkhead and extrusion that limited access to the root. Samples taken from location 3 clearly show that the weld throat rupture initiates at this lack of root fusion defect and leads to tearing through the entire weld throat under the bending action of the bulkhead during topple testing.

4 GRW Assessment of Rim Joints

GRW undertook a structural strength study to provide a comparison between the GRW rim joint design and the informative joint design provided in Figure D.15(a) of BS EN 13094:2008 (BSI, 2008). Their numerical analyses comprised plane strain finite element models of various rim joint geometries with the bulkhead subjected to pure, in-plane bending. This is illustrated in Figure O11. Two conclusions from this document were:

- The single-sided fillet weld rim joint design (ie that of Period A tankers) is sensitive to the throat thickness. Should the single-sided fillet weld's throat be too small, it is predicted that the weld will start to tear from the weld root through the weld throat.
- It is predicted that the plate (bulkhead) will start to tear at the inner surface of the bulkhead and that the tear will propagate through the plate thickness due to the plastic strain reaching 20% at this location first.

The conclusion related to the throat-thickness for single-sided fillet weld rim joints does not provide a specific value of throat thickness that is too small. However, the rim joint welds from J2580 (a Period A tanker) had throat thickness typically in excess of 5.0mm. The fracture of the J2580 rim joint weld did not arise due to the presence of plastic strains alone, but was most likely due to an existing 3.0mm lack of root fusion defect.

Whilst the second conclusion provides insight into the potential cause of the observed failures, the explanation is insufficient to completely characterise the failures. This is because the ruptures occurred at the ends of the flattened portion of the end dish and not near the middle of the flattened portion where the (in-plane) bending was most extreme.

5 Analytical Assessment of Rim Joint Rupture

5.1 Overview

Finite element analysis was undertaken to provide a supplementary explanation for the parent metal ruptures observed in the end dish of J3910 after topple testing based.

5.2 Objective

- To use finite element analysis to provide an explanation for the rim joint ruptures observed after topple testing.

In this appendix, the numerical analyses undertaken to assess the rim joint ruptures have been performed in an informative way. Specifically, the dynamic conditions of the topple test have not been exactly replicated in the model and the geometry does not precisely represent a particular band (ie an end dish or interior circumferential band). As discussed in the HSL report (2014), after topple testing, it was revealed that all compartments failed leak-proof testing. Therefore, although additional sectioning of the interior bands and bulkheads/baffles has not yet been undertaken, it is possible that all bands exhibited similar ruptures, leading to inter-compartment leaks. Thus, the objective of this section of the appendix is to provide an analytical means to predict these failures, whilst not focussing on the specific geometry of a circumferential joint or the specific dynamic characteristics of the topple test.

5.3 Geometry

A three-dimensional model was created to represent a typical, circumferential extrusion band-to-bulkhead joint. The extrusion profile was assumed to be that of Period B and Period C tankers, ie the extrusion band is joined to the bulkhead by a double-sided fillet weld and does not feature the additional up-stand to position the bulkhead (ie Figure O12 as opposed to Figure O10). The bulkhead and extrusion band geometry assumed an elliptical shape with horizontal, semi-major axis length 1250mm and vertical, semi-minor axis length 825mm. The dome-shaped bulkhead had a maximum overhang of 225mm (see Figure O12) and was 6mm thick. A small amount of 5mm wall thickness tanker shell was joined to the extrusion band on the side of the extrusion band opposite to the overhang of the bulkhead. The fillet welds between the extrusion band and the bulkhead were modelled with approximately 5mm weld throats. The slot for the bulkhead was not modelled and no additional imperfections such as axial misalignment were included. A single circumferential weld (idealised to join the tanker shell to the bulkhead) was modelled with a 1.25mm weld cap height. The bulkhead was modelled almost entirely with quadratic, reduced integration, shell elements (type S8R in Abaqus) to facilitate faster computation times and better resolution of the anticipated large bending strains and large rotations. The rest of the geometry was modelled with solid parts and quadratic, reduced integration brick elements (type C3D20R in Abaqus). The mesh was designed to be fine within the rim joint region and all elements had a uniform circumferential length of 10mm. Several images of the geometry are shown in Figure O12 and of the finite element mesh in Figure O13.

A Cartesian coordinate system was employed with the z-axis aligned with the axis of the circumferential joint and the plane x=0 passing through the 6 o'clock (bottom) and 12 o'clock (top) positions of the tanker. Quarter symmetry was employed due to symmetry considerations with respect to the geometry and loading. Whilst this does not identically represent the geometry of a circumferential extrusion band-to-bulkhead joint of a GRW tanker (due to the shape not being truly elliptical and other geometrical simplifications employed),

it is sufficient to provide a means for analysing the failures observed after topple testing.

5.4 Material properties

The elastic-plastic tensile properties employed in the finite element model are those as described in the main report.

5.5 Loads and boundary conditions

Loads and boundary conditions were defined in a way to represent the deformation that the circumferential joint experiences during topple testing. To that end, the ground was represented by a flat, rigid, analytical part and was kinematically coupled to a single, centrally-positioned reference node. This node was restrained in all degrees of freedom except for the y (up-down) degree of freedom. A displacement in the positive y-direction was applied to the reference node until sufficient deformation of the joint geometry was obtained as described in Section 5.6. To react against the movement of the ground, the top surface of the quarter-symmetry geometry was restrained in the y-direction. Additionally, the end faces of the tanker shell (ie the faces parallel to the z=0 plane) were restrained in the z- (axial) direction. Finally, to represent the longitudinal symmetry plane, all nodes located on the plane x=0 were restrained in the x-direction. The displacement of the ground was applied statically, ie no inertial effects were included in the simulation. The loads and boundary conditions are illustrated in Figure O12. The finite strain formulation was employed due to the large displacements in the simulation, and the contact between the ground and the tanker geometry was defined as hard, normal contact with a tangential penalty friction coefficient of 0.1. The displacement of the ground was applied in small increments to ensure convergence and equilibrium tolerances were met.

This definition of loads and boundary conditions essentially represents the static crushing of the tanker between two rigid plates. Whilst the dynamic aspects and fluid-structure interaction features of the topple test have not been included, the results indicate that this model provides a suitable means of studying the deformation of the tanker experienced during topple testing.

5.6 Results

The simulation was analysed until the flattened length of the extrusion band model exceed 425mm. Taking into account symmetry conditions, this represented a total flattened length of 850mm. The flattened length was assessed by monitoring the contact pressure variable (CPRESS in Abaqus). The position furthest from the longitudinal symmetry plane with a non-zero value of contact pressure was taken to represent the extent of the region of the extrusion band that was in contact with the ground and hence "flattened" (see Figure O14). For each solution increment, the displacements, principal strains, plastic strains and stresses were output. As the simulation was analysed under the finite strain formulation, the strains were calculated as logarithmic strains.

Several images of the deformation of the model are shown in Figure O15 and Figure O16. In Figure O16, to view the shell elements of the bulkhead from the side, the total shell element thickness has been plotted. However, due to certain rendering tolerances of shell elements in Abaqus (particularly under finite strain formulation where transverse shear is included), this has resulted in the lines that represent the shell surfaces appearing discontinuous with the solid elements. This is only a feature of the image rendering and not representative of any error in the finite element model.

5.7 Discussion

Qualitatively, the deformation of the end dish from J3910 after topple testing agrees very well with the deformation observed in the finite element model. For example:

- The middle of the flattened portion exhibits larger in-plane bending than the ends of the flattened portion.
- The overall shape of the non-linear bulge/buckle of the end dish in the model closely resembles the images of the J3910 section received by TWI for metallographic examination.

In order to assess the propensity for a fracture failure somewhere along the rim joint, the concept of a forming limit diagram has been employed. A forming limit diagram (FLD) provides a graphical description of material failure tests such as biaxial tension tests and punched dome tests. The diagram is comprised of a "safe" region and an "unsafe" region separated by the forming limit curve. The forming limit curve is defined as a locus of points with x-coordinate minor strain and y-coordinate major strain. FLDs are typically employed in the sheet metal forming industry to determine the propensity for cracks to appear during forming. Due to the thin nature of sheets, the through-wall strains are negligible, and therefore the strain state at any given point can be wholly described by the minor and major principal strains. For the present analysis, the large span of the bulkhead compared with its thickness enables the forming limit diagram approach to be used. A literature review of FLDs for Al 5182-O, the aluminium alloy of the bulkhead, was undertaken to provide an approximate forming limit curve suitable for the present analysis (Abedarabbo et al, 2005; Soare, 2007; Li, 2011). Whilst FLDs have some dependency on strain-rate, thickness, temperature, heat treatment and pre-strain, a lower-bound curve, obtained from the literature review, was employed based upon FLDs for samples that were described in the references as "as-received". The results obtained from this forming limit curve have provided reasonable comparisons to the topple test results, and therefore these additional dependencies had only secondary influences.

The HSL report on the topple tests (2014) indicates that after testing, the flattened length of the end dish was between 700mm and 800mm. Therefore, from the TWI finite element model, two solution increments were identified: one with flattened (total) length approximately 800mm and one with flattened (total) length approximately 720mm. For each of these solution increments, a circumferential path of nodes was defined, approximately 2.0mm offset from the toe of the rim joint weld (ie the toe of the fillet weld joining the extrusion band to the bulkhead on the bulkhead side). This path is shown in Figure O17. At each node in this path, the minimum principal strain (minor strain) and maximum principal strain (major strain) were extracted. The reason for taking the 2.0mm offset was because of the loss of accuracy that can occur for nodal extrapolation of strains at a geometrically-sharp weld toe. Additionally, the cracking in J3910 was not located identically at the weld toe but was offset by a small amount. The extracted strains were then plotted on the forming limit diagram obtained from the literature review. The results are shown in Figure O18.

In Figure O18, it can be seen that when the flattened length is 720mm long, all points lie below the forming limit curve and therefore, for the geometry considered, rupture is not predicted to occur. However, when the flattened length is 800mm long, seven nodes lie above the failure assessment curve. Since the circumferential spacing of the nodes in the finite element model was

10mm, this means that the model predicts an approximately 70mm long rupture to occur. The nodes that are located above the forming limit curve are positioned precisely at the end of the flattened portion, ie at the end of the bulge. This is where the ruptures occurred in parent metal/bulkhead of J3910. In particular, as can be seen in Figure O2, the ruptures at the ends of the bulge of the end dish of J3910 were approximately 70-100mm long. Therefore, independently of the geometric approximation in the finite element model and the potential variability of the forming limit curve used, the present FEA provides an analytical method to explain the ruptures that occur in J3910 after the topple test.

6 Conclusions

In this appendix, the metallographic examinations of the rim joints after topple testing of J3910 and J2580 have been described. The numerical analyses undertaken by GRW in relation to the rim joint performance were reviewed, and additionally supplementary analyses were performed by TWI to provide an explanation for the failures. It was observed that:

- In J2580, the rupture occurred through the weld throat of the rim joint weld. The most probable explanation for this event was a lack of root fusion defect that was present due to the combination of the fit up between the bulkhead and extrusion band slot and the presence of a welding start/stop position or overlap.
- In J3910, the ruptures occurred in the bulk head. Whilst GRW provided numerical analyses that indicated ruptures of this sort would occur under pure, in-plane bending of the bulkhead, their analyses did not accurately describe the position of the ruptures, or lack thereof. By employing a three-dimensional model, qualitatively similar to the topple test, and using the concept of a forming limit diagram, the ruptures at the ends of the bulge were explained. The primary difference between the TWI and GRW analyses and conclusions was the inclusion of biaxiality effects in the TWI finite element model

7 References

Abedarabbo N, Pourboghrat F, and Carsley J, 2005: 'Forming of AA5182 and AA5754-O at elevated temperatures using coupled thermo-mechanical finite element models', International Journal of Plasticity, Vol 23, pp 841-875.

GRW, 2014: 'End dish weld joint structural comparison: ADR examples vs GRW detail', Report No PVVR20140008, Revision 0. Report Date: 31 October 2014.

HSL, 2014: 'Technical assessment of petroleum road fuel tankers. Work Package 1 – Full scale testing and associated modelling. Tanker topple test methods and results. Document ES/14/39/04rev05, 2014.

BSI, 2008: IS EN 13094:2008 'Tanks for the transport of dangerous goods – Metallic tanks with a working pressure not exceeding 0.5bar – Design and construction', British Standards Institution, 2008.

Li J, 2011: 'Characterization of post-annealing mechanical behaviour of preformed aluminium alloy 5182-O', PhD Dissertation, Department of Mechanical Engineering, University of Michigan, 2011.

Soare S, 2007: 'On the use of homogeneous polynomials to develop anisotropic yield functions with applications to sheet forming', PhD Dissertation, University of Florida, 2007.

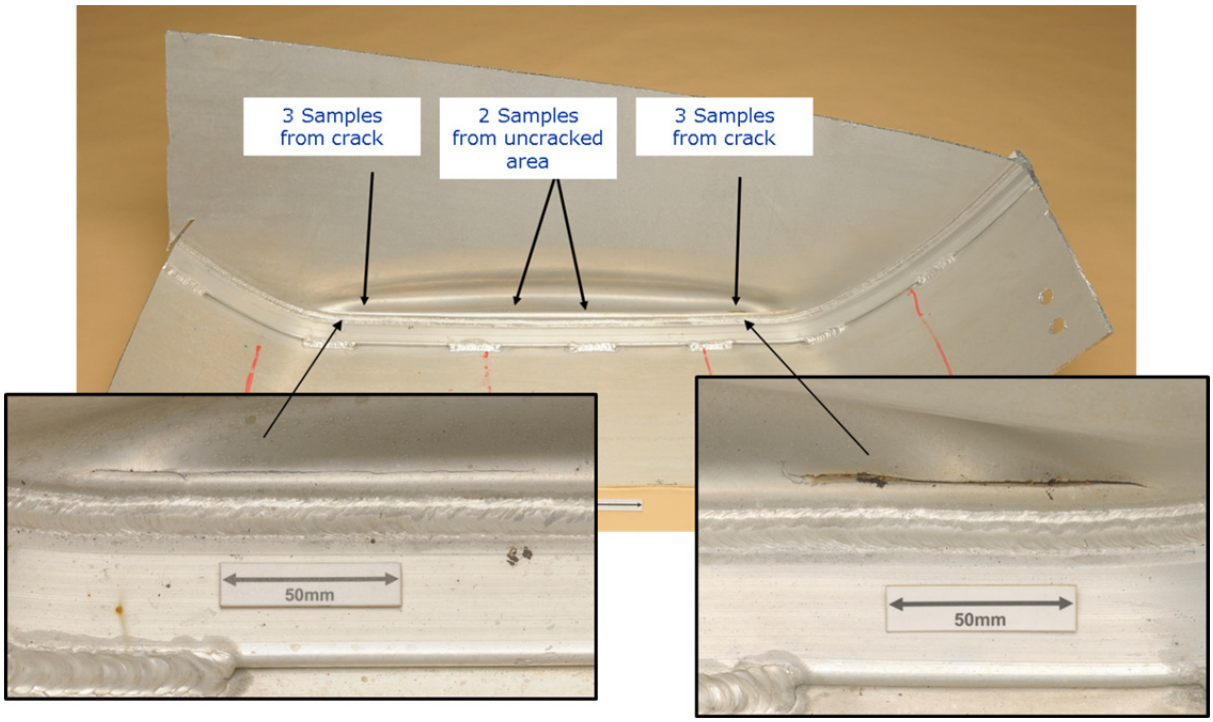

Figure O1 Image of the entire J3910 section as-received by TWI.

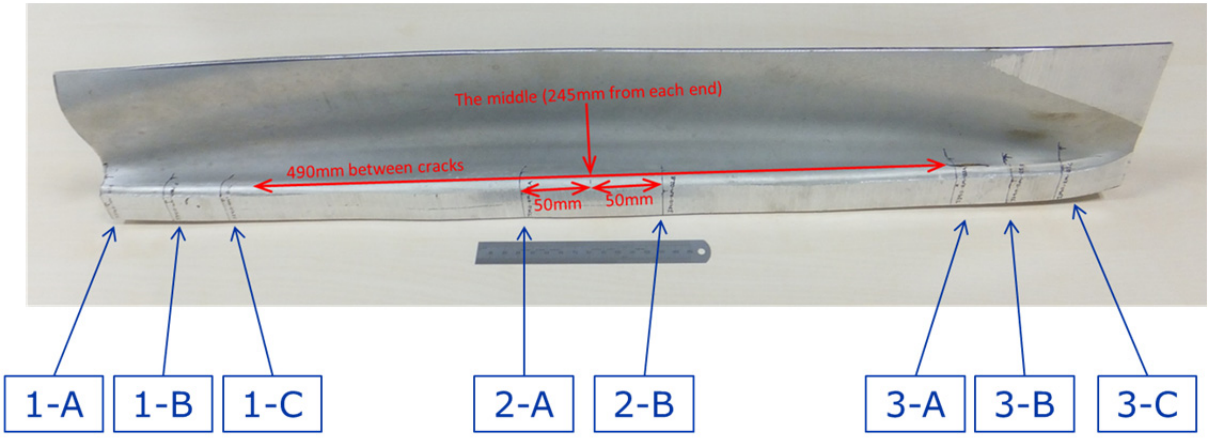

Figure O2 Image of the J3910 end dish and identification of sample locations.

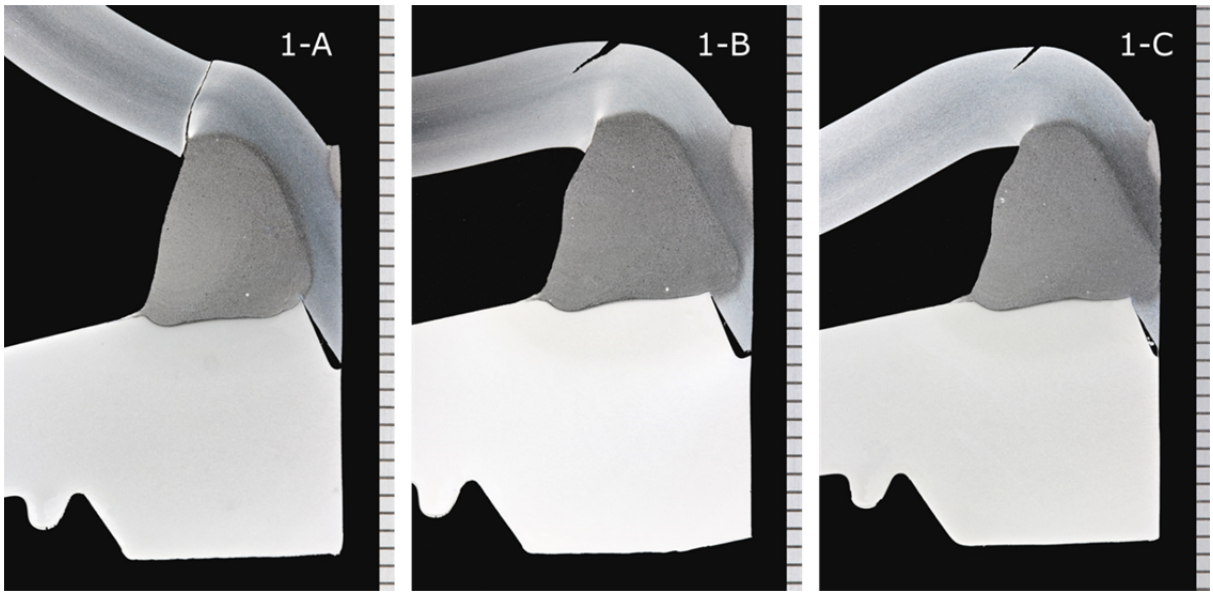

Figure O3 Samples 1-A, 1-B and 1-C taken from J3910. Note the level of curvature (bending strain) in 1-A compared with 1-C. The tick marks indicate a 1mm length.

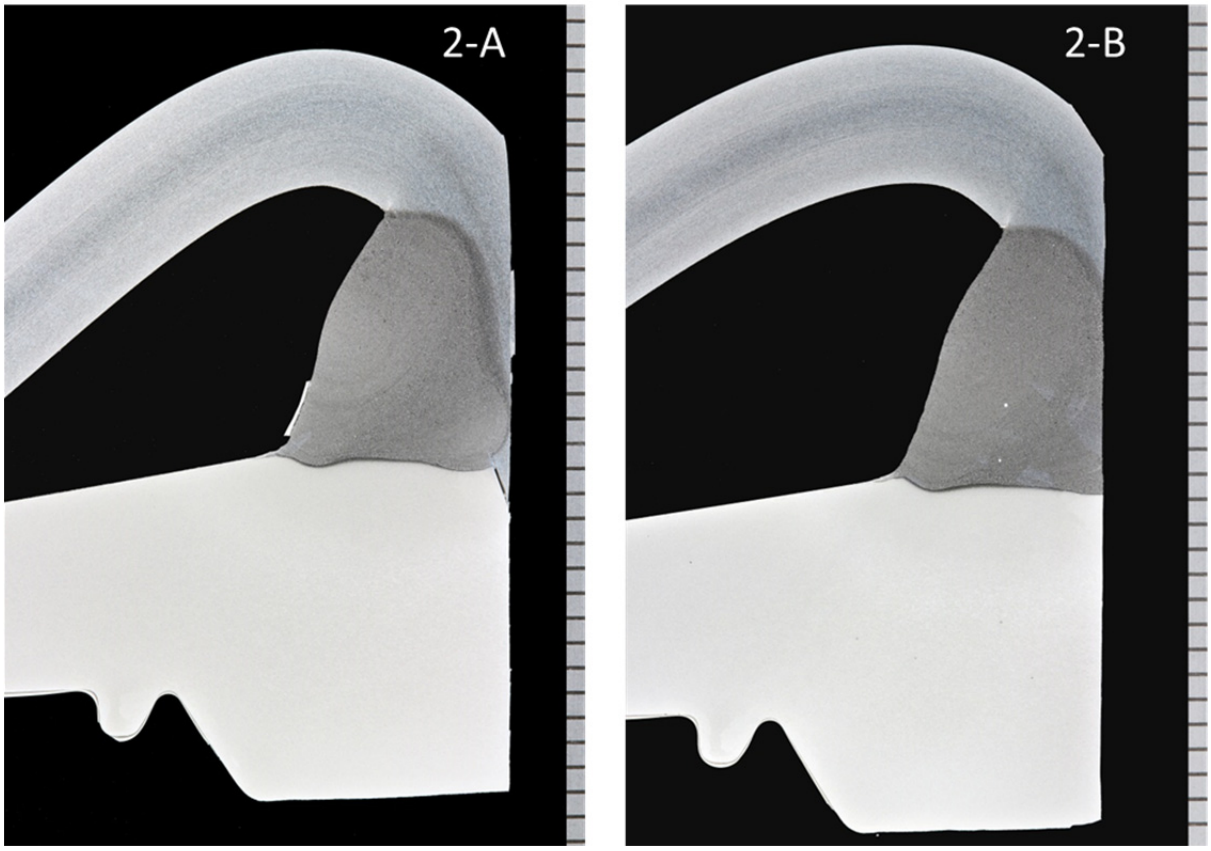

Figure O4 Samples 2-A and 2-B taken from the centre of the flattened portion of J3910. Note the extent of in-plane bending and absence of cracking. The tick marks indicate a 1mm length.

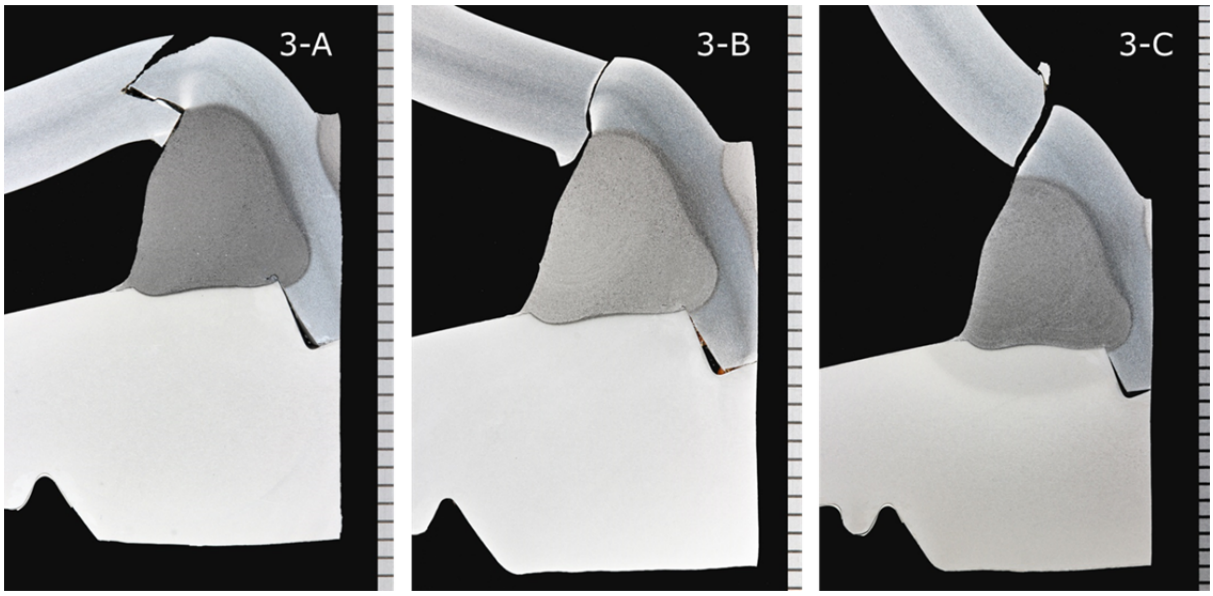

Figure O5 Samples 3-A, 3-B and 3-C from J3910. All samples exhiibit rupture through the bulkhead/end dish.

Figure O6 Image of the entire section of J2580 received by TWI with the locations of sampling illustrated.

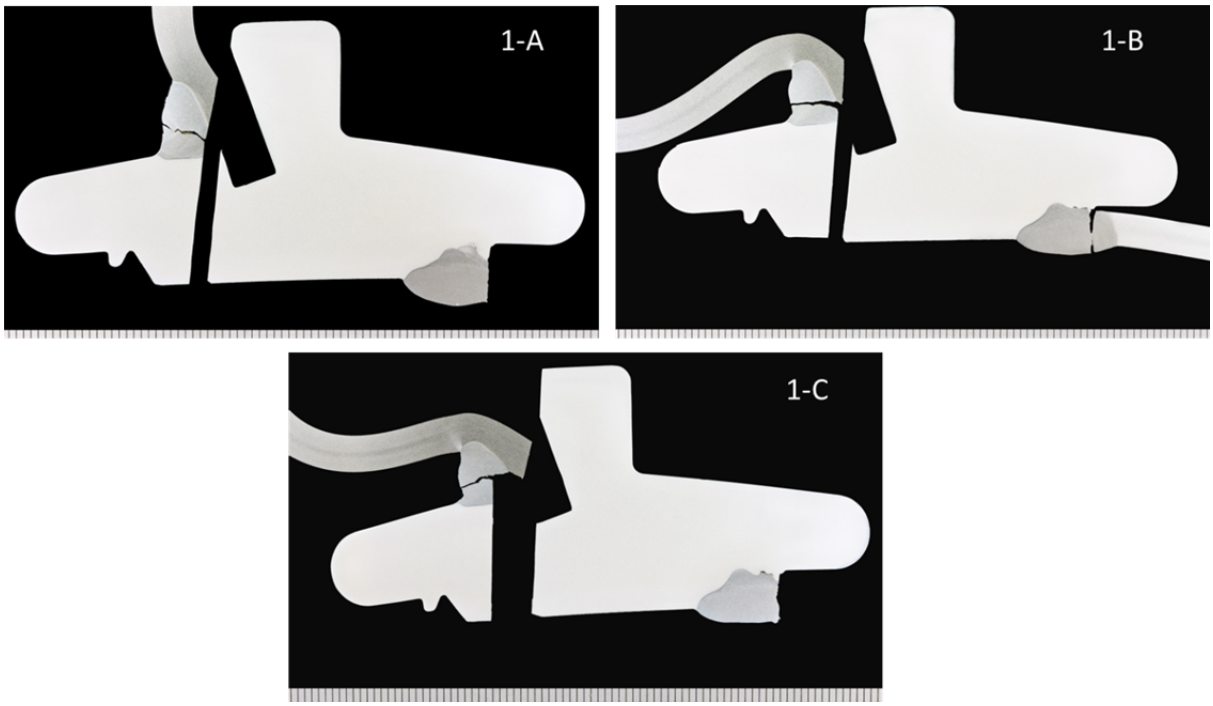

Figure O7 Samples 1-A, 1-B and 1-C from J2580. The large parallel gap is due to machining of the samples for previous examination of the circumferential weld. All samples show rupture through the weld throat. The tick marks indicate 1.0mm scale.

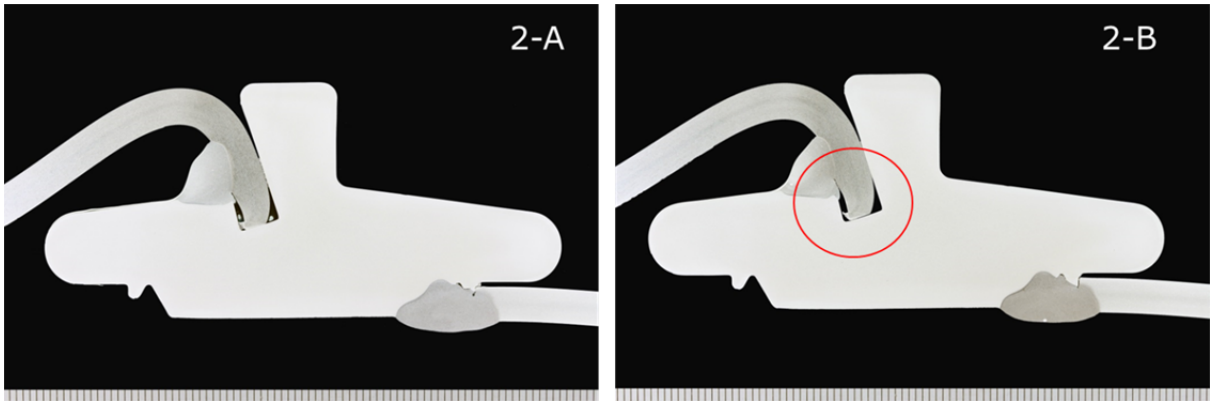

Figure O8 Samples 2-A and 2-B from the centre of the flattend portion of the section from J2580. Note the level of in-plane bending and absence of cracking. The tick marks indicate 1.0mm scale.

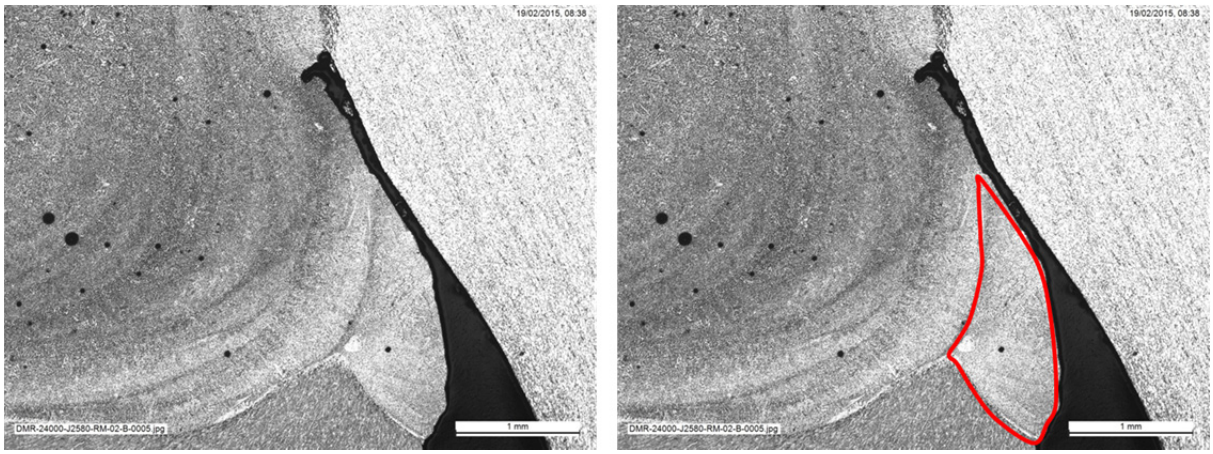

Figure O9 Micrograph of the rim joint weld for sample 2-B from J2580. On the right frame, the red contour encloses the apparent previous weld pass or start-stop welding position. The length scale is 1.0mm.

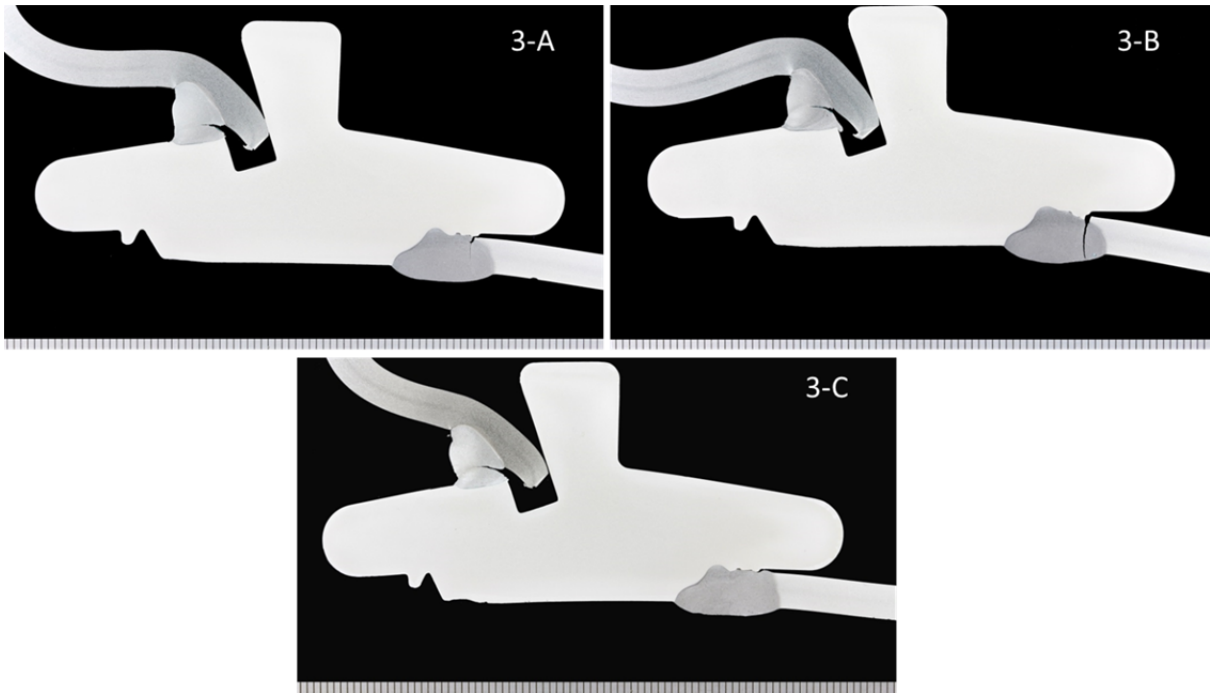

Figure O10 Samples 3-A, 3-B and 3-C from J2580. Sample 3-B shows both the weld throat cracking and the circumferential weld cracking. All samples show various stages of weld throat rupture of the rim joint weld.

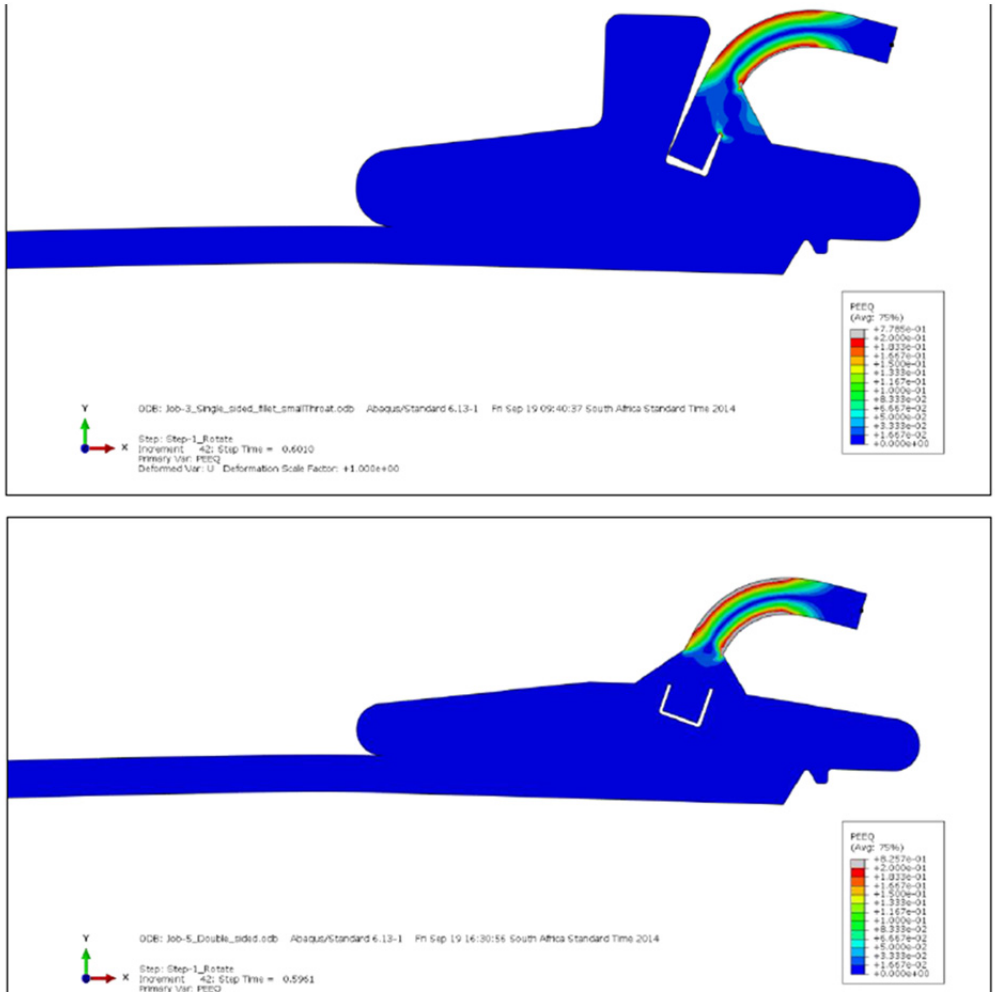

Figure O11 Images of the GRW finite element model. Top frame is Figure 2 and bottom frame is Figure 3 from the report by GRW (2014).

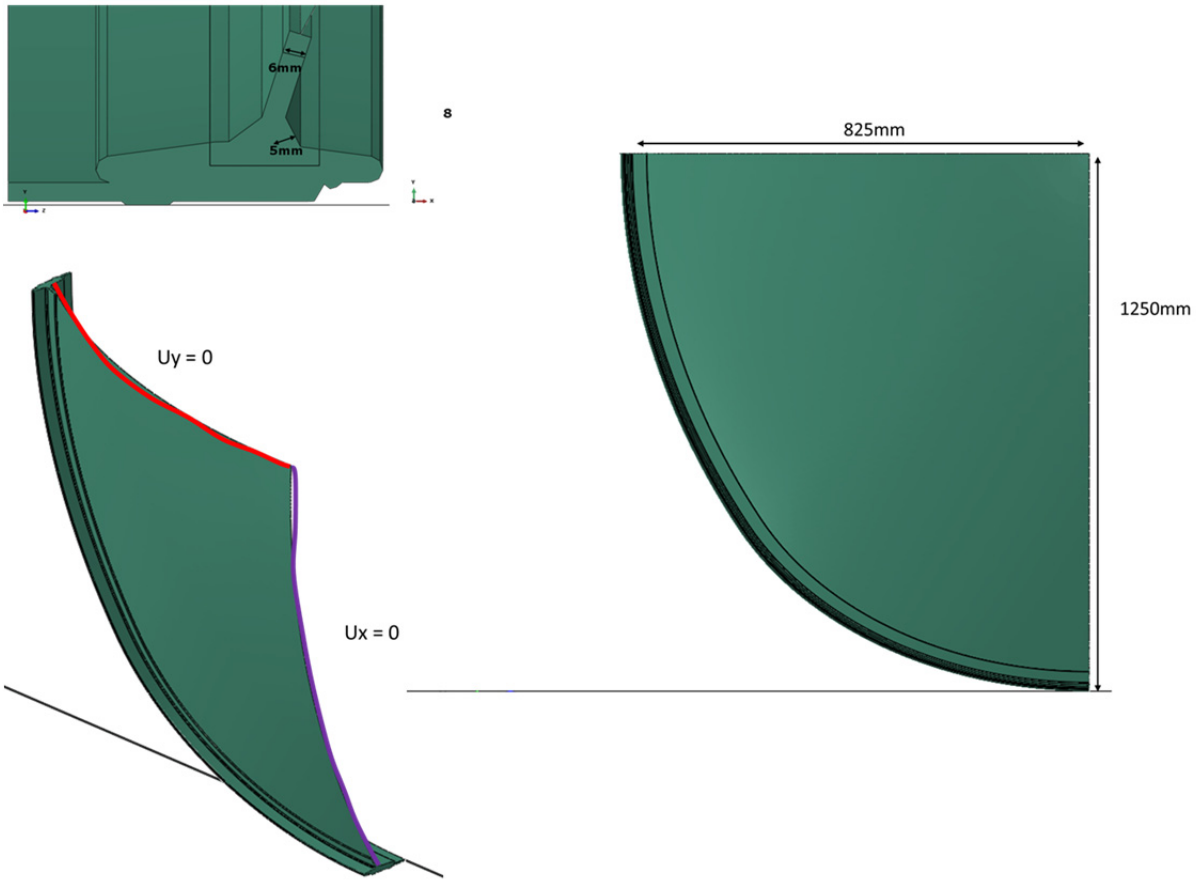

Figure O12 Geometry of the TWI finite element model used to analyse the bulkhead rupture during topple testing.

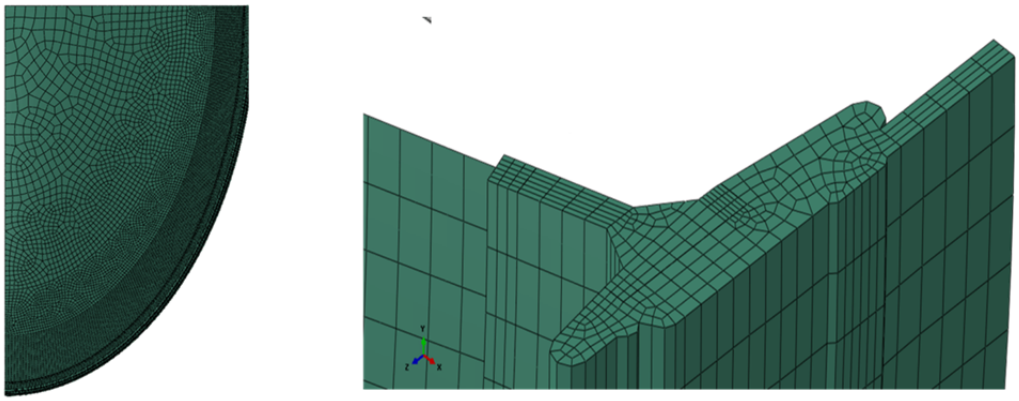

Figure O13 Finite element mesh of the TWI model used to analyse the bulkhead rupture during topple testing. The main portion of the bulkhead has been modelled with shell elements.

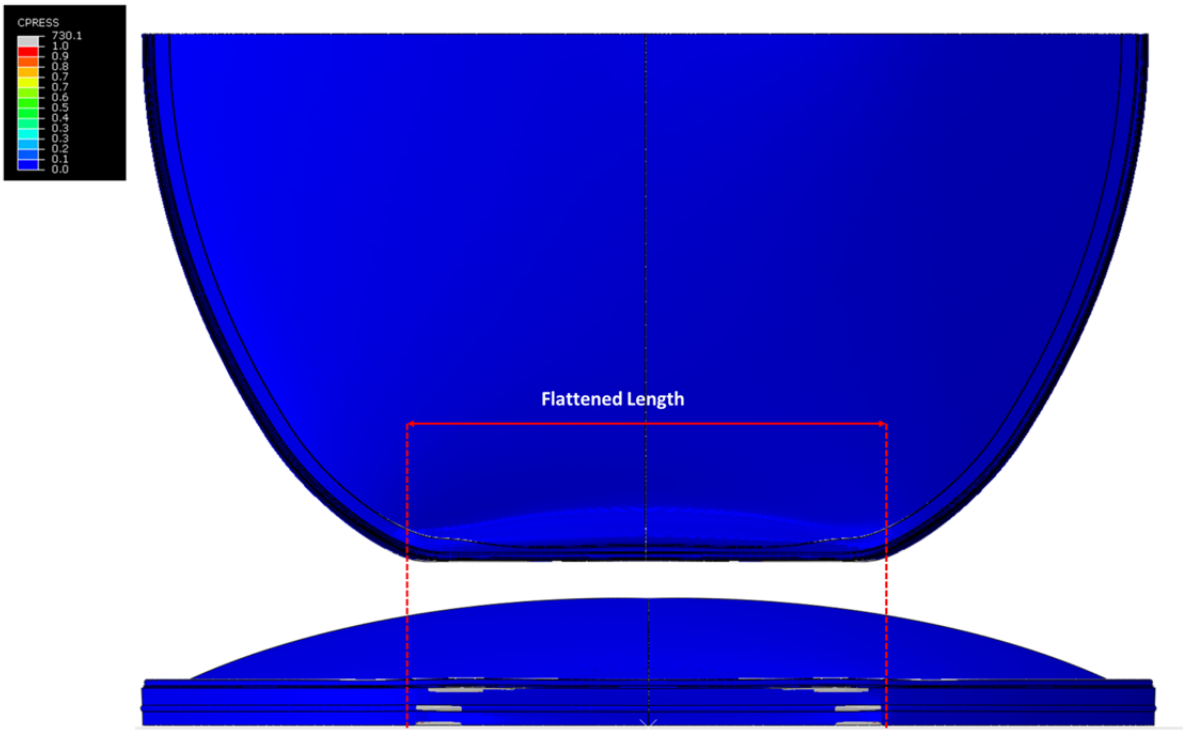

Figure O14 Illustration of the contact pressure variable used to identify the flattened length. In the lower frame of this figure, the bottom surface of the extrusion profile is shown (as viewed from the bottom) where grey colours indicate the presence of contact.

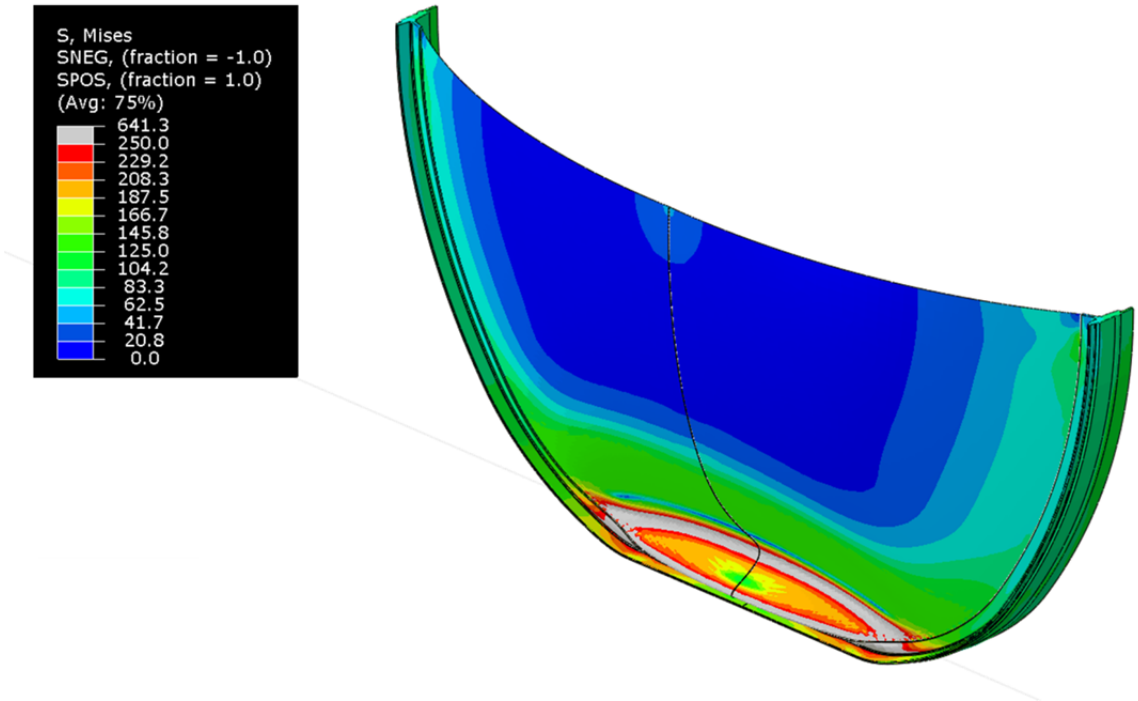

Figure O15 Von Mises stress contours for the rim joint assessment model.

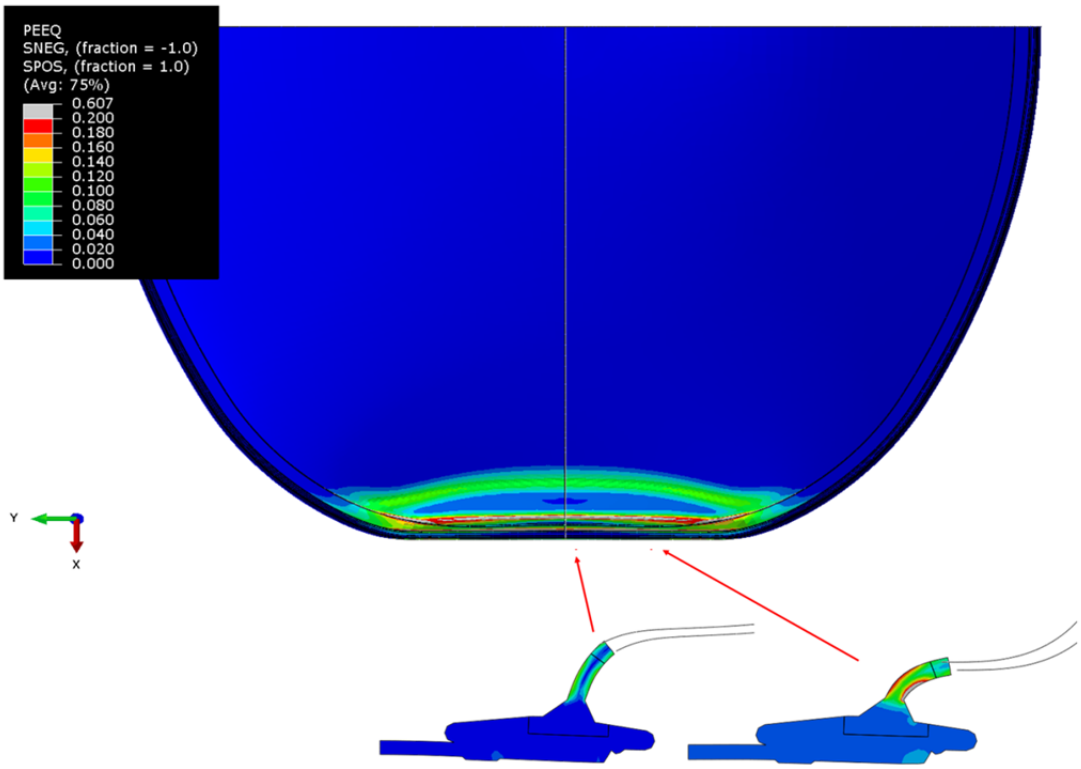

Figure O16 Illustration of the different in-plane deformation for the rim joint assessment model. The plastic strain (PEEQ) contour has been plotted with a slice of the joint at the symmetry plane (left frame, showing more significant in-plane bending of the bulge) and 400mm offset (right frame).

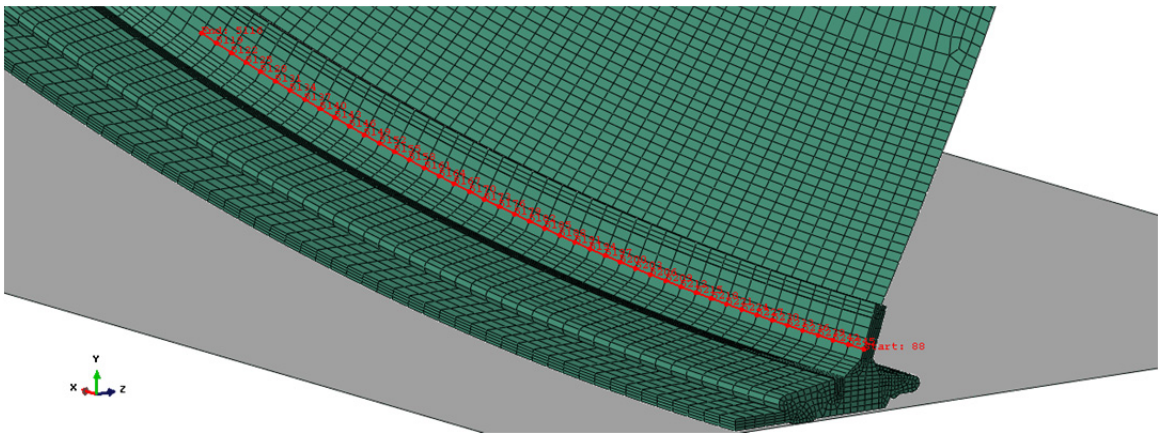

Figure O17 Diagram of the path used for extraction of minor and major strains.

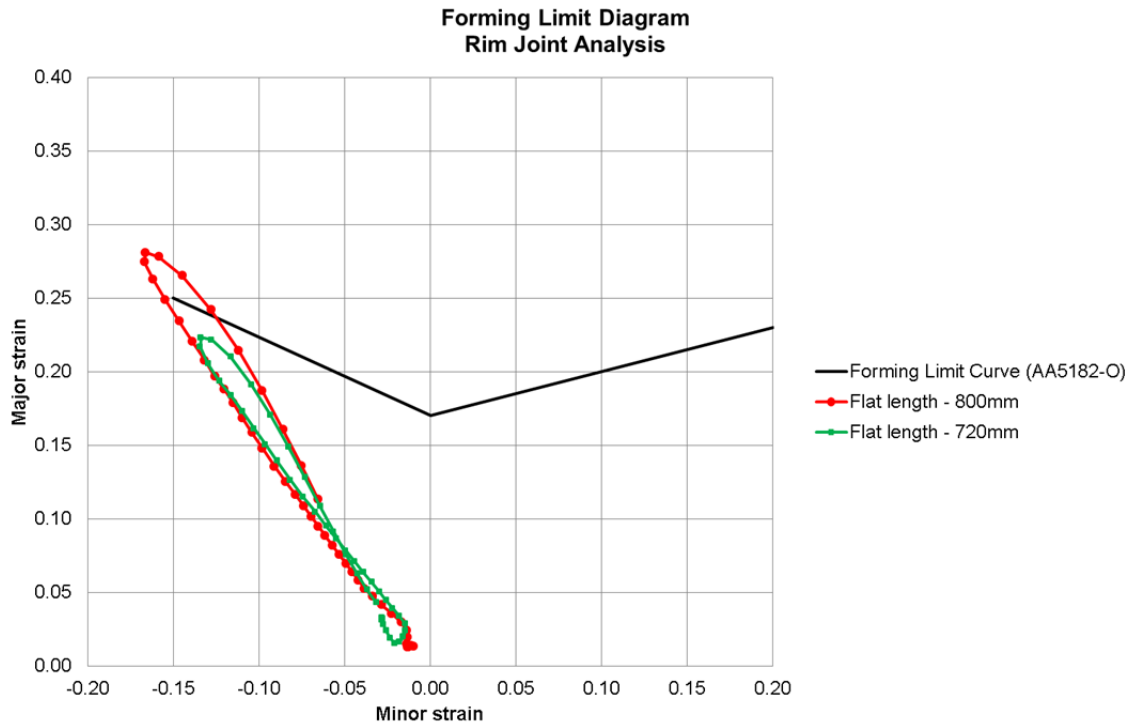

Figure O18 Forming limit diagram showing the assessment of the formability of the bulkhead around the circumference.